Performance of a feedback-controlled, deterministic source of single chromium atoms

Shannon B. Hill and Jabez J. McClelland

Electron Physics Group, National Institute of Standards and Technology, Gaithersburg, Maryland 20899-8412

Received July 7, 2003; revised manuscript received October 21, 2003; accepted October 22, 2003

A magneto-optical trap with feedback-controlled loading and loss rates is used to realize a deterministic source of single chromium atoms with single-atom occupation probability as high as 0.987 ± 0.001. We present a series of measurements of the performance of this source and discuss the dependence of the probability of not having a single atom in the trap (error rate) on experimental parameters. We describe a simple analytical model that considers mean load rate, trap lifetime, stray load rate, and feedback response time, and we also present results of Monte Carlo calculations that take into account all experimental conditions. We find that the analytical model describes the behavior well for error rates as small as about 0.03, but the Monte Carlo simulations must be used to model behavior at error rates lower than this, as the occupation probability approaches unity.

OCIS codes: 020.7010, 020.5580.

1. INTRODUCTION

Since the earliest experiments with atomic beams at the beginning of the 20th century, the vast majority of studies on atomic interactions with photons, electrons, other atoms, or molecules have been conducted under conditions where the arrival of atoms in the interaction region is completely random. Recently, however, there has been an intensifying interest in studies in which single, isolated atoms need to be under complete experimental control, both in location and arrival time. These studies are motivated in part by new developments in quantum engineering, where proposed quantum information architectures require unprecedented control over isolated quantum systems, and also by a need for a deeper understanding of fundamental processes such as atom–atom interactions, cavity quantum electrodynamics, and parity nonconservation effects. Further motivation comes from nanotechnology, where ever-shrinking nanoscale devices are rapidly approaching the atomic scale, and deterministic placement of single atoms is becoming a necessity.

As a way to address the needs of these new studies, we recently developed a deterministic source of Cr atoms capable of producing single atoms "on demand."[1] We showed that a single atom can be made available for extraction at essentially any time with a measured probability of nearly 0.99, and also that single atoms can be ejected periodically at rates approaching 10 Hz while maintaining the probability of ejecting a single atom at a level of 0.90 or higher. Our deterministic atom source is based on a magneto-optical trap (MOT) for Cr with fluorescence detection efficiency high enough to detect easily the fluorescence of a single atom. This high detection efficiency permits real-time feedback control over the trap loading and loss rates at the single atom level. In essence, loading is turned on only if the fluorescence falls below the single atom level, and the trap is dumped if the fluorescence goes above the single atom level.

While our source of atoms is unique in its use of feedback to attain an unprecedented degree of determinism, it was developed in the context of a number of earlier and ongoing single-atom studies based on MOTs. Hu and Kimble,[2] Ruschewitz *et al.*,[3] and Haubrich *et al.*[4] observed single atoms in a MOT, showing it is possible to discern clearly the random loading and loss of single atoms. These pioneering studies have been extended recently by Frese *et al.*,[5] Kuhr *et al.*,[6] and Schrader *et al.*,[7] who demonstrated the deterministic extraction of a single atom from a randomly loaded MOT with a long trap lifetime. Also, Schlosser *et al.*[8] used a MOT to capture atoms in a very tight dipole trap, where they saw a reduction in the probability of having more than one atom as a result of collisional effects. All of these studies rely on stochastic processes to produce single atoms, and thus require relatively long, random waiting times before a single atom is made available. In contrast, the focus of our work is to create a source capable of repeatedly producing single atoms when and where they are desired at as fast a rate as possible.

In this paper, we present a series of measurements of the performance of our feedback-controlled, single-atom MOT and compare these measurements with predictions of simple analytical models based on general Poissonian load–loss processes and with Monte Carlo simulations that take into account all the details of the experimental conditions. We discuss the performance in terms of an error rate, which is defined as the probability of *not* finding a single atom in the MOT at a given instant. We find that the simple analytical models describe the performance very well as long as the error rate is higher than about 0.03 (single-atom probability $\leqslant 0.97$). On the other hand, the lowest error levels obtained—as small as

0.013—are not well reproduced by the analytical models, but are very well described by Monte Carlo simulations.

2. EXPERIMENT

The experiments described here were conducted in a Cr MOT apparatus optimized for low background scattered light and high fluorescence detection efficiency. The vacuum chamber consisted of a central cylindrical section nominally 200 mm in diameter and 100 mm long. On this chamber were mounted two reentrant flanges holding the magnetic field coils for the MOT (36 turns of water-cooled, 3.2-mm-diameter copper tubing each with mean radius 19 mm and separation 33 mm), four radial arms holding antireflection-coated viewports at a distance of approximately 390 mm from the chamber center, and two axial arms holding antireflection-coated viewports at distances of 210 mm and 420 mm from the chamber center. The long distances between the viewports and the chamber center were chosen to minimize the detection of stray light scattered as the MOT beams passed through the viewport glass. Additional measures taken to minimize scatter included tilting of the viewports 5° off normal to direct the residual backreflected beams onto cone-shaped baffles and placement of apertures in the radial arms where they connected to the chamber. To further reduce light scatter, the cones and apertures were blackened by application of soot from a butane flame. The chamber was pumped by two ion pumps, and had a typical residual gas pressure of $(0.5\text{ to }1.0)\times 10^{-6}$ Pa [$(4\text{ to }8)\times 10^{-9}$ Torr].

The MOT was formed in the standard way[9] with six circularly polarized laser beams directed along the two axial and four radial directions of the chamber, and a magnetic field gradient of 0.75–0.85 $\mathrm{T\,m^{-1}}$. Laser light was provided by a UV-pumped, stilbene-3 dye laser tuned just below the $^7S_3 \rightarrow {}^7P_4^\circ$ transition in Cr at 425.6 nm. The laser beams typically had $1/e^2$ diameters of 4–7 mm and powers of 22 ± 8 mW (radial beams) and 7 ± 3 mW (axial beams).[10] Because the $^7P_4^\circ$ level in Cr has two slow decay channels to the metastable $^5D_3$ and $^5D_4$ levels (lifetimes of 24 ms and 8 ms, respectively[11]), two repumping laser beams were directed continuously at the MOT to ensure a closed optical pumping cycle.[12,13] These repumping beams were supplied by two grating-stabilized diode lasers, one tuned to the $^5D_3 \rightarrow {}^7P_4^\circ$ transition at 649.2 nm, the other to the $^5D_4 \rightarrow {}^7P_4^\circ$ transition at 658.3 nm (see Fig. 1). The intensities of these beams at the MOT were 200–700 $\mathrm{W\,cm^{-2}}$ and (600–2200) $\mathrm{W\,cm^{-2}}$, respectively. The frequency of the MOT laser was locked to a saturable absorption signal from a hollow-cathode cell with magnetic field tuning, and the repumping laser frequencies were locked in reference to a frequency-stabilized HeNe laser by way of a scanning etalon.[14]

Fluorescence from the MOT was collected by a pair of back-to-back achromatic lenses (focal lengths 50.8 mm and 200 mm) mounted in a reentrant viewport at a distance of 46 mm from the center of the vacuum chamber. The lenses had a clear aperture of 23 mm diameter, so fluorescence into a solid angle of 0.2 sr was collected. The magnification of this optical system was 3.89 and the resolution was measured to be better than 5 μm at the object plane. We note that this resolution is an important factor in suppressing stray light detection because it allows a small aperture to be used at the image plane. We found that an optimum signal-to-background ratio was obtained with a 200-μm-diameter aperture. After passing through the aperture, the fluorescence light was filtered by a 425-nm interference filter and was detected with a single-photon-counting photomultiplier with NaK cathode. Measurements of the optical system showed a net transmission of ≈40%. Combining this with the manufacturer-specified photomultiplier quantum efficiency of ≈16%, we estimate a net quantum efficiency of 6.4%. Based on this quantum efficiency and the solid angle of the collection optics, we found that the observed single-atom photon count rates were in agreement with what was expected for single-atom fluorescence.

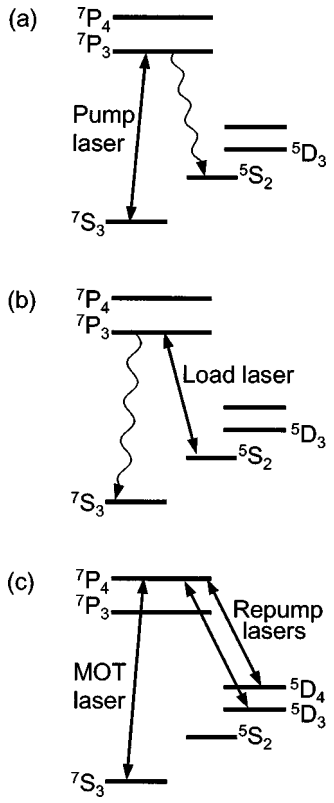

Fig. 1. Energy levels of Cr showing the laser transitions used to control loading and trap the atoms (vertical distances not to scale). (a) Atoms are collimated, deflected and transferred to the metastable $^5S_2$ level with a pump laser tuned to the $^7S_3 \rightarrow {}^7P_3^\circ$ transition at 427.6 nm. (b) When loading is desired, atoms are repumped to the ground state with a load laser tuned to the $^5S_2 \rightarrow {}^7P_3^\circ$ transition at 633.2 nm. (c) Atoms are trapped with a laser tuned to the $^7S_3 \rightarrow {}^7P_4^\circ$ transition at 425.6 nm and repumped by two lasers tuned to the $^5D_3 \rightarrow {}^7P_4^\circ$ and $^5D_4 \rightarrow {}^7P_4^\circ$ transitions at 649.2 nm and 658.3 nm, respectively.

Cr atoms were supplied by a resistively heated commercial effusion cell operating at a temperature between 1200 °C and 1400 °C and located approximately 370 mm below the MOT in an auxiliary chamber. No Zeeman slower was used to load the MOT since the required flux of trappable atoms at the MOT was quite modest. However, to achieve fast switching on and off of the loading, an optical pumping scheme was implemented (see Figs. 1

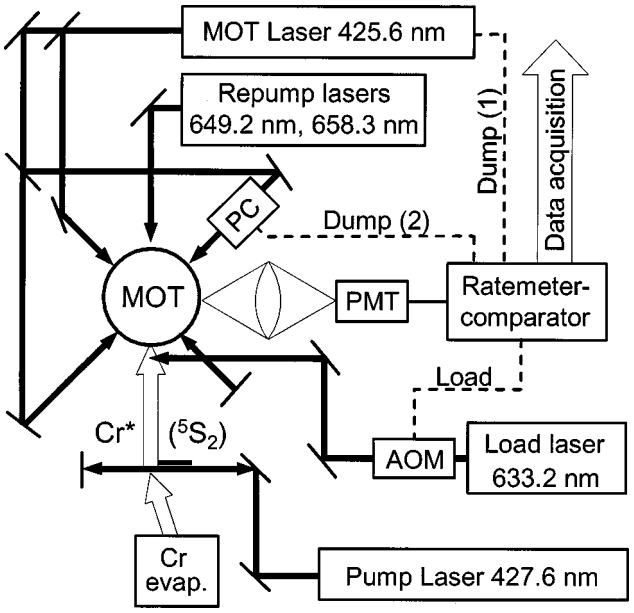

Fig. 2. Schematic of the experiment. Cr atoms produced in an evaporator are collimated, deflected and transferred to the metastable $^5S_2$ level with a pump laser. A load laser, switched by an acousto-optic modulator AOM repumps atoms to the ground state for loading. Fluorescence from the MOT is collected by a photomultiplier PMT, the output of which is averaged in a rate meter and fed into a comparator. A load signal controls the load laser AOM, and a dump signal controls either (1) the detuning of the MOT laser or (2) a Pockels cell PC on one of the MOT beams.

and 2). In essence, the line of sight from the Cr cell to the MOT was blocked while a population of slow atoms was collimated, deflected back toward the MOT, and optically pumped into a metastable state. Just before the MOT, another laser beam optically pumped atoms back into the ground state when loading was required.

Line of sight from the Cr cell was blocked by a movable flag located 255 mm below the MOT. A few millimeters below this flag, collimation, deflection, and optical pumping to the $^5S_2$ level were accomplished by a laser beam (pump laser) retroreflected across the atom beam. This laser beam, arising from a second UV-pumped, stilbene-3 dye laser, was tuned just below the $^7S_3 \rightarrow {}^7P_3^\circ$ transition in Cr, where laser cooling and deflection took place as atoms cycled on this transition until they decayed from the $^7P_3^\circ$ level to the metastable $^5S_2$ level with a lifetime of 34 μs.[15] By optimizing the interaction length, power, and detuning of the pumping laser, essentially all ground-state atoms that were deflected toward the MOT and were going slowly enough to be captured could be transferred to the $^5S_2$ level. Typically an interaction length of 25 ± 5 mm and laser powers of 50–130 mW were used. Detuning of this laser was not measured, but rather optimized operationally. Its frequency was locked by monitoring fluorescence in an auxiliary Cr beam with a split photodiode.[16,17]

The laser beam used to control loading of the MOT (load laser) was supplied by another grating-stabilized diode laser tuned to the $^5S_2 \rightarrow {}^7P_3^\circ$ transition in Cr at 633.2 nm and frequency-locked to the same scanning etalon as the repumping lasers. Its power was 1.0 ± 0.1 mW and its $1/e^2$ diameter was 0.1–0.2 mm. Loading control was effected by switching this laser beam on and off with an acousto-optic modulator. Because of the close proximity of this laser beam to the MOT (approximately 1 mm), any loading delay was dominated by the time required for deceleration of the atom during the capture process.

Dumping of the MOT, necessary in cases when more than one atom was loaded by chance, was accomplished for most of the measurements presented here by simultaneously blocking one of the MOT radial beams with a Pockels cell and turning off the magnetic field. Because it was desirable to empty the MOT as quickly as possible both of these actions were necessary, and we found that the unbalanced light force of the MOT in combination with the removal of any magnetic trapping potential was most effective for this. For a few of the measurements, the MOT laser frequency was briefly shifted just above resonance as an alternate dumping mechanism. In all cases, the dumping condition was maintained for approximately 5 ms during which time loading was kept off. This was necessary to ensure the atom(s) had time to leave the MOT region.

Signal processing for feedback control of the MOT population at the single-atom level proceeded as follows. The pulse train from the photomultiplier was fed into a rate meter that produced an analog output with adjustable time constant. The output from this rate meter was then fed into a two-channel comparator. If the fluorescence level fell below a preset single-atom threshold, a logic signal from the first channel turned on loading by activating the acousto-optic modulator. If the fluorescence level rose above a preset two-atom threshold, a logic signal from the second channel activated the dump process. The rate meter time constant and the load and dump thresholds were the main adjustable parameters in the feedback loop, and values were chosen to obtain optimum performance based on measurements and simulations.

3. MODELS

In this section we present a simple analytical model that describes the performance of the feedback-controlled MOT well over a large range of parameters, and we also discuss full Monte Carlo simulations that take into account all experimental parameters.

A. Analytical Model

A relatively simple picture of the feedback-controlled MOT performance can be obtained by taking a probabilistic approach and considering the system to have two states: The MOT either has a single atom (state 1), with probability P_1, or it does not (state 0), with probability $P_0 = 1 - P_1$. We are interested in deriving an expression for P_0, which we call the error rate for the system. Very generally, if we assume random transition processes between state 0 and state 1 that do not depend on P_0 and P_1, we can write a differential equation describing the time evolution of P_0:

$$\frac{dP_0}{dt} = -T_{0\rightarrow 1}P_0 + T_{1\rightarrow 0}P_1, \tag{1}$$

where $T_{0\to1}$ ($T_{1\to0}$) is the probability of making a transition from 0 to 1 (1 to 0) per unit time. In steady state, we can set the time derivative to zero and solve for P_0:

$$P_0 = \frac{T_{1\to0}}{T_{1\to0} + T_{0\to1}}. \tag{2}$$

Equation (2) can now be used to derive an expression for P_0 in terms of MOT parameters. We begin by assuming that the feedback is perfect—that is, the system responds instantaneously—and the only perturbation to the MOT population is random loss (due, for example, to background gas collisions) with a rate ${\tau_{\mathrm{MOT}}}^{-1}$, where τ_{MOT} is the MOT lifetime. Further, we assume that when loading is turned on, atoms load randomly with a mean rate R_{load}. Based on these assumptions, we can write $T_{0\to1} = R_{\mathrm{load}}$ and $T_{1\to0} = {\tau_{\mathrm{MOT}}}^{-1}$. Note that the assumption of perfect feedback allows us to ignore the situation in which the MOT has more than one atom because a perfect dump will instantaneously change this state to one with no atoms. Thus we can write

$$P_0 = \frac{1}{1+\lambda} \qquad \text{perfect feedback}, \tag{3}$$

where we define $\lambda \equiv R_{\mathrm{load}}\tau_{\mathrm{MOT}}$. We express P_0 in terms of the dimensionless quantity λ because it makes the expression very simple, and also because it provides a connection to the single-atom occupation probability of a MOT with no feedback. In such a randomly loaded MOT, the only parameters governing the population are the mean rates R_{load} and ${\tau_{\mathrm{MOT}}}^{-1}$ associated with the Poissonian load and loss processes. Accordingly, the probability of having a single atom in the MOT is determined by Poisson statistics to be $\lambda\exp(-\lambda)$, giving

$$P_0 = 1 - \lambda\exp(-\lambda) \qquad \text{no feedback}. \tag{4}$$

We note that while the error rate for a no-feedback MOT can never be smaller than 0.63, the perfect-feedback MOT can have an infinitely small error rate.

Of course, perfect feedback is an idealized situation and any real feedback-controlled MOT will have some degree of error. It is, in fact, one of the purposes of this study to examine the errors that do occur and explore the extent to which they can be minimized. We have found that the inclusion of only two additional effects in our simple model provides excellent agreement with experiment for all but the smallest error rates.

The first of these is a stray-loading rate R_{stray} that represents undesired loading of additional atoms when there is already a single atom in the trap. This can arise, for example, from incomplete optical pumping of the atoms into the $^5S_2$ metastable state, or simply from random slow Cr atoms that may be present in the vacuum chamber. In our experiment R_{stray} was quite small but was not completely negligible. We can account for R_{stray} in our model by noting that a stray loading event in effect causes a transition from state 1 to state 0, assuming the dump is completely efficient. Thus we write

$$T_{1\to0} = {\tau_{\mathrm{MOT}}}^{-1} + R_{\mathrm{stray}} \qquad (R_{\mathrm{stray}} \ll R_{\mathrm{load}}). \tag{5}$$

The second effect is a nonnegligible probability of loading more than a single atom when loading is turned on due to a finite response time in the feedback loop. This effect, which becomes significant only when the load rate becomes comparable to or greater than the inverse of the response time, can be modeled by modifying the expression for $T_{0\to1}$. In order for the system to truly load only one atom, it is necessary to load a single atom and then maintain this state throughout the response time of the feedback loop τ_{resp} without loading another atom. If another atom loads during this time period, the system is returned immediately to state 0, assuming again that the dump is perfect. If we assume the loading is governed by a Poisson process, we can replace the instantaneous rate $T_{0\to1}$ with a rate that is in effect averaged over the response time:

$$T_{0\to1} \to R_{\mathrm{load}}\exp(-R_{\mathrm{load}}\tau_{\mathrm{resp}}). \tag{6}$$

Here, we have multiplied the load rate by the probability of surviving a time τ_{resp} without a load event $\exp(-R_{\mathrm{load}}\tau_{\mathrm{resp}})$ to give the true single-atom loading rate.

Combining Eq. (5) and relation (6) with Eq. (2), we write

$$P_0 = \frac{1 + R_{\mathrm{stray}}\tau_{\mathrm{MOT}}}{1 + R_{\mathrm{stray}}\tau_{\mathrm{MOT}} + \lambda\exp(-R_{\mathrm{load}}\tau_{\mathrm{resp}})}. \tag{7}$$

Equation (7) provides a simple analytic expression for P_0 that, as will be seen below, makes quite good predictions for the performance of the feedback-controlled MOT. We note that for small values of R_{stray} and τ_{resp}, Eq. (7) reverts to Eq. (3), as expected.

Assuming this simple model is applicable, it is of interest to answer some simple questions about the best choice of parameters for operating the feedback-controlled MOT with minimum error rate. For example, if we assume R_{stray}, τ_{MOT}, and τ_{resp} are fixed, we may wish to know what value of R_{load} gives the best performance. Minimization of Eq. (7) shows that we should choose $R_{\mathrm{load}} = {\tau_{\mathrm{resp}}}^{-1}$, whereupon the optimum value for P_0 becomes

$$P_0^{\mathrm{opt}} = \frac{1 + R_{\mathrm{stray}}\tau_{\mathrm{MOT}}}{1 + R_{\mathrm{stray}}\tau_{\mathrm{MOT}} + \tau_{\mathrm{MOT}}{\tau_{\mathrm{resp}}}^{-1}e^{-1}}. \tag{8}$$

Given this minimum value for P_0, we might ask which parameters would be the most fruitful to improve or modify if a smaller error rate were desired. Clearly, the smaller we make τ_{resp} and R_{stray}, the better the performance will be. For given values of τ_{resp} and R_{stray}, however, the performance improves only asymptotically with larger τ_{MOT}, approaching a constant value for very large MOT lifetimes:

$$\lim_{\tau_{\mathrm{MOT}}\to\infty} P_0^{\mathrm{opt}} = \frac{eR_{\mathrm{stray}}\tau_{\mathrm{resp}}}{1 + eR_{\mathrm{stray}}\tau_{\mathrm{resp}}}. \tag{9}$$

While the minimization of R_{stray} is relatively straightforward, improvement of τ_{resp} means examining its two most significant constituents, the rate meter time constant τ_{meas} and the time lag τ_{lag} between when an atom destined for capture leaves the load laser region and when it actually appears in the MOT. Though τ_{meas} can be shortened by reducing the time constant on the rate meter, it cannot be reduced indefinitely because of statistical noise in the fluorescence signal. A lower bound is

set by the mean single-atom-fluorescence detection rate Γ_{atom} and the average background photon rate Γ_{bkgnd}. Together with τ_{meas}, these rates determine the statistical fluctuations $\sqrt{(\Gamma_{\mathrm{atom}} + \Gamma_{\mathrm{bkgnd}})/\tau_{\mathrm{meas}}}$, of the total detected photon rate which must be smaller than Γ_{atom} to clearly resolve individual atoms in the MOT. Minimization of τ_{lag} is accomplished by recognizing that it is largely governed by the time needed for deceleration as the atom is trapped, plus any additional time of flight needed to traverse the distance from the load laser region to the MOT. Essentially, the MOT parameters and the geometry of the apparatus must be arranged to make these as small as possible.

B. Monte Carlo Model

The analytical model discussed above provides insight into the qualitative behavior of the feedback-controlled MOT and makes reasonably accurate predictions, provided the error rate is not too low, but it neglects a number of effects that become significant as the performance is pushed to its limit. In particular, it does not take into account the delays and feedback control errors produced by the counting statistics of the fluorescence and background signals, which play an ever-increasing role as τ_{meas} is reduced to speed up the feedback response. In addition, it does not explicitly include the threshold levels used in the loading and dump controls, nor does it include the finite time required for a dumping event to ensure the trap is emptied. One consequence of these omissions is an improper modeling of the load and dump process when the load rate is high. In the experiments, and in the Monte Carlo simulations discussed below, we observe that the load and dump gates interact at high load rates, sometimes causing a chattering effect that is a result of repeated overloading and dumping. This phenomenon is neither predicted nor included in the analytical model.

To provide a model that mimics experimental conditions as precisely as possible and also allows us to make predictions about performance under any conditions, we use a Monte Carlo simulation that follows the time evolution of the MOT population by breaking the entire time period of the simulation into time steps dt small compared with all time scales involved. We explicitly include the fluorescence signal from the MOT and the background signal as independent Poisson-distributed streams of pulses with mean rate $n\Gamma_{\mathrm{atom}}$ (n is the number of atoms in the trap) and Γ_{bkgnd}, respectively. The intentional loading (when turned on) and the stray loading of atoms are also treated as independent Poisson processes with mean rates R_{load} and R_{stray}, respectively. Since the number of atoms in the trap is generally small, the loss from the trap is treated as a binomial process, assuming the n atoms in the trap behave independently and can each be lost with probability $1 - \exp(-dt/\tau_{\mathrm{MOT}})$. At each time step we choose a random number of emitted photons from a Poisson distribution with mean rate determined by the number of atoms in the trap, the fluorescence rate per atom Γ_{atom}, and the background scatter rate Γ_{bkgnd}. This photon number is exponentially averaged with time constant τ_{meas}, and a decision is made to load atoms, do nothing, or dump the trap, based on the value of the averaged fluorescence signal relative to predefined load and dump thresholds, and on whether a lag time or a dump delay time has expired. Random numbers are then chosen for the number of atoms loaded and lost from the trap based on the appropriate distributions. A fluorescence signal is calculated for the resulting new number of atoms in the trap, and the procedure is repeated until the entire time sequence is calculated. Statistics are maintained for the amount of time spent with 0, 1, 2... atoms in the trap, and the error rate is calculated as $1 - P_1$, where P_1 is the fraction of the total time spent with exactly one atom in the trap.

4. RESULTS

To explore the behavior of our feedback-controlled MOT, we conducted a series of measurements of the error rate during which all parameters that affect the performance were monitored. Using the measured values of the parameters, we were able to predict the performance with both the analytical model and the Monte Carlo model and compare the predictions with the observations.

A measurement consisted of collecting fluorescence from the feedback-controlled MOT for a period of 200 s and analyzing the data for the amount of time spent in the single-atom state. Under typical experimental conditions, the average photon rate per atom was $\approx$3500 s^{-1} and the background scatter rate was $\approx$200 s^{-1}. The rate meter time constant τ_{meas} was set to 5 ms, the load threshold was set to $\approx$1050 s^{-1}, and the dump threshold was set to $\approx$7300 s^{-1}.[18] The dump delay (the time allowed for the atom to be ejected from the trap) was set to 5 ms.

Runs were conducted at a range of different oven temperatures to observe how the performance varied for different load rates. For each run, Γ_{atom} and Γ_{bkgnd} were extracted from the fluorescence time series by fitting a function consisting of two Poisson distributions to a histogram of the data. R_{load} was measured by examining every loading event during a run and determining the average length of time the loading gate was on before a single atom was loaded. For the runs presented here, R_{load} ranged from 0.9 s^{-1} to 115 s^{-1}, depending on the oven temperature. The lag time τ_{lag} was measured independently to be 4 ± 2 ms by observing the delay in the onset of MOT fluorescence at a very high load rate. R_{load} was not corrected for τ_{lag} because the correction was insignificant at the load rates used. R_{stray} was estimated by measuring the mean time interval between MOT dumps that were triggered by the stray loading of a second atom. It generally increased with R_{load} and had values between 0.005 s^{-1} and 0.235 s^{-1}. τ_{MOT} was measured by first determining the average survival time in the single-atom state τ_{single} and then correcting for stray loading (which would give the appearance of a shorter trap lifetime) using the relationship $\tau_{\mathrm{MOT}} = (\tau_{\mathrm{single}}{}^{-1} - R_{\mathrm{stray}})^{-1}$. We found that τ_{MOT} varied from run to run over a fairly large range, from 0.9 s to 5.2 s. We attribute this to the trap lifetime's being very sensitive to the frequency stability of the repumping lasers, which tended to vary from day to day. While we cannot completely rule out the possibility that the lifetime drifted during the course of a run, we have some confidence that it was con-

stant for any given run because successive runs conducted on a single day tended to have similar lifetimes, whereas runs conducted on different days tended to have different lifetimes.

For each run, we extracted the error rate P_0 from the fluorescence time series data. To do this we defined fluorescence levels, based on the single atom fluorescence rate and background scatter rate, above and below which we could say the MOT contained a single atom. To guard against statistical fluctuations in the fluorescence signal giving false readings, we also required that the signal remain above or below the specified level for at least twice the rate meter time constant. We then added up the total amount of time spent in the single-atom state t_{single} and calculated $P_0 = 1 - t_{\text{single}}/t_{\text{total}}$, where t_{total} is the total run time.

In Fig. 3 we show measured values of P_0 for a number of runs conducted at different oven temperatures. Instead of plotting the data versus R_{load}, we use the parameter $\lambda = R_{\text{load}}\tau_{\text{MOT}}$ as the abscissa. We choose this method of displaying the data because this tends to bring runs with differing values of τ_{MOT} onto a single line, as one would expect based on the analytical models discussed above. To indicate the magnitude of τ_{MOT} for each measurement, the data are plotted with symbol size and gray level proportional to τ_{MOT}. Uncertainty estimates displayed in Fig. 3 as error bars were obtained by determining the standard deviations associated with the measurement uncertainty and the statistical sampling uncertainty. These were then combined in quadrature to give overall one-standard-deviation uncertainties.

Also plotted in Fig. 3 for comparison with the experiments are the error rate expected with no feedback [Eq. (4)], the perfect feedback model [Eq. (3)], and the analytical model of Eq. (7). For the analytical model, we calculated a value of P_0 at each measured value of λ by using the measured values of R_{stray} for each point and an estimated value for τ_{resp} of $\tau_{\text{meas}} + \tau_{\text{lag}} = 9.3\,\text{ms}$. As can be seen, the perfect feedback limit predicts the behavior well up until $\lambda \approx 10$. For the experiments conducted in this regime, $R_{\text{load}}\tau_{\text{resp}} \ll 1$ and $R_{\text{stray}}\tau_{\text{MOT}} \ll 1$, so this model is appropriate. Between $\lambda = 10$ and $\lambda = 100$, however, there is significant deviation between the data and the perfect model. Here, we see that the analytical model of Eq. (7), which takes into account stray loading and feedback loop response time, does an excellent job in predicting the behavior.

At the lowest error rates, which were obtained above $\lambda \approx 100$, we see that the analytical model does not reproduce the measurements well. In this regime, the performance depends critically on all the experimental parameters, and an analytical model has limited usefulness. In Fig. 4 we show these low-error-rate measurements along with results of the Monte Carlo simulations discussed above. The data are plotted as a function of run number, as each run represents a unique combination of experimental parameters, and no single parameter or combination of parameters dominates the behavior. The parameters for each run, along with the results, are tabulated in Table 1. The measurements are shown as filled circles with error bars to indicate one-standard-deviation uncertainties, while the simulation results are plotted as gray bars whose height corresponds to plus and minus one-standard deviation of ten simulations calculated for each set of conditions. Figure 4 shows excellent agreement between the simulations and experiment, indicating that when all conditions are included in our model, predictions can be made with confidence.

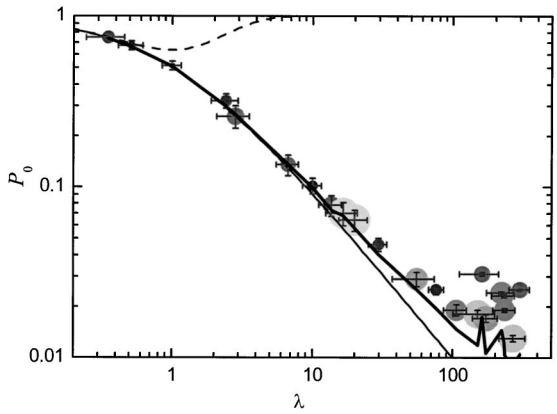

Fig. 3. Error rate P_0, or probability of *not* having a single atom in the MOT, as a function of $\lambda = R_{\text{load}}\tau_{\text{MOT}}$, the product of the load rate and the MOT lifetime. The filled circles indicate measurements with the symbol size and gray level proportional to τ_{MOT}, which ranges from 0.9 to 5.2 s. The light solid curve represents the perfect feedback model of Eq. (3), the dark solid curve represents the analytical model of Eq. (7), and the dashed curve shows the behavior with no feedback. Error bars indicate one-standard-deviation uncertainties as discussed in the text.

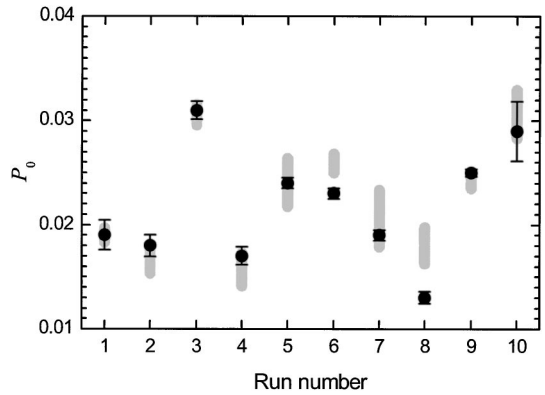

Fig. 4. Error rate P_0, or probability of *not* having a single atom in the MOT, plotted as a function of run number. The circles indicate the same measurements as those shown in Fig. (3) with $\lambda > 100$. Error bars indicate one-standard-deviation uncertainties for these measurements, as discussed in the text. The gray bars indicate Monte Carlo calculations, for which the height of the bar corresponds to plus and minus one-standard deviation of 10 simulations in each case. The experimental parameters corresponding to the indicated run numbers are shown in Table 1.

5. CONCLUSIONS

We have made measurements of the performance of a deterministic source of single atoms using a feedback-controlled MOT and compared these measurements with predictions of analytical and Monte Carlo models. Agreement between experiment and the analytical models is good when the error rate is above about 0.03, while the Monte Carlo model is found to capture all the essential physics even at the lowest error rates.

Table 1. Run Parameters for Data Presented in Fig. 4

Run no.	Single-Atom Fluorescence, s^{-1}	Background, s^{-1}	Load Threshold, s^{-1}	Dump Threshold, s^{-1}	R_{load}, s^{-1}	τ_{MOT}, s	R_{stray}, s^{-1}
1	3590[a]	180[a]	1000	7000	30.2 ± 3.4[b]	3.5 ± 0.5[b]	0.05 ± 0.02[b]
2	3650	220	1000	7200	32.3 ± 3.8	4.6 ± 1.4	0.07 ± 0.02
3	3330	260	1000	7200	61.4 ± 6.8	2.6 ± 0.8	0.23 ± 0.05
4	3400	240	1000	7200	42.1 ± 4.4	4.1 ± 0.7	0.06 ± 0.02
5	3570	220	1000	7000	61.3 ± 3.8	3.6 ± 0.8	0.24 ± 0.02
6	3410	300	1000	7200	74.2 ± 4.6	3.1 ± 0.6	0.14 ± 0.03
7	3320	290	1000	7200	67.4 ± 5.1	3.5 ± 0.6	0.09 ± 0.02
8	3550	350	1142	7670	58.7 ± 5.2	4.6 ± 0.9	0.09 ± 0.02
9	3440	350	1000	7200	115.1 ± 6.1	2.6 ± 0.4	0.08 ± 0.02
10	3760	170	1000	7200	14.8 ± 1.4	3.8 ± 1.2	0.07 ± 0.02

[a] Single-atom fluorescence and background rates were calculated by averaging over an entire 200 s run. The one-standard deviation uncertainty for these values is less than 10 s^{-1} for a given run. Variation from run to run is larger than this because of slight changes in experimental conditions between runs.

[b] Uncertainties for R_{load}, τ_{MOT}, and R_{stray} are one standard deviation and are derived as described in the text.

In this paper we have concentrated on the probability of *not* finding a single atom in the trap, or error rate, as a metric of performance because it predicts the usefulness of the source for applications where it is necessary to have a single atom on demand at an arbitrary time. A related metric is the single-atom-success probability when atoms are extracted at a fixed rate. We have also found that our Monte Carlo simulation does very well in predicting the behavior of the source in this situation.[1] The success of the Monte Carlo simulations in all situations, along with the ability of the analytical models to predict behavior in the appropriate regimes, gives us confidence in our understanding of the behavior of the feedback-controlled MOT as a single-atom source. This confidence will allow us to predict and optimize the behavior for specific applications, such as a deterministic source of atoms for quantum information processing, or deterministic doping of nanostructures.

ACKNOWLEDGMENTS

The authors wish to thank Robert Celotta, Mark Stiles, Stefan Leigh, James Yen, Andrew Rukhin, and the members of the National Institute of Standards and Technology Electron Physics Group for thoughtful discussions and technical support.

Corresponding author J. McClelland's e-mail address is jabez.mcclelland@nist.gov.

REFERENCES AND NOTES

1. S. B. Hill and J. J. McClelland, "Atoms on demand: Fast, deterministic production of single Cr atoms," Appl. Phys. Lett. **82**, 3128–3130 (2003).
2. Z. Hu and H. J. Kimble, "Observation of a single atom in a magneto-optical trap," Opt. Lett. **19**, 1888–1890 (1994).
3. F. Ruschewitz, D. Bettermann, J. L. Peng, and W. Ertmer, "Statistical investigations on single trapped neutral atoms," Europhys. Lett. **34**, 651–656 (1996).
4. D. Haubrich, H. Schadwinkel, F. Strauch, B. Ueberholz, R. Wynands, and D. Meschede, "Observation of individual neutral atoms in magnetic and magneto-optical traps," Europhys. Lett. **34**, 663–668 (1996).
5. D. Frese, B. Ueberholz, S. Kuhr, W. Alt, D. Schrader, V. Gomer, and D. Meschede, "Single atoms in an optical dipole trap: towards a deterministic source of cold atoms," Phys. Rev. Lett. **85**, 3777–3780 (2000).
6. S. Kuhr, W. Alt, D. Schrader, M. Müller, V. Gomer, and D. Meschede, "Deterministic delivery of a single atom," Science **293**, 278–280 (2001).
7. D. Schrader, S. Kuhr, W. Alt, M. Muller, V. Gomer, and D. Meschede, "An optical conveyor belt for single neutral atoms," Appl. Phys. B **73**, 819–824 (2001).
8. N. Schlosser, G. Reymond, I. Protsenko, and P. Grangier, "Sub-Poissonian loading of single atoms in a microscopic dipole trap," Nature (London) **411**, 1024–1027 (2001).
9. E. L. Raab, M. Prentiss, A. Cable, S. Chu, and D. E. Pritchard, "Trapping of neutral sodium atoms with radiation pressure," Phys. Rev. Lett. **59**, 2631–2634 (1987).
10. Unless otherwise stated, all ± uncertainties cited in this paper are intended to be interpreted as one-standard-deviation combined random and systematic uncertainties.
11. J. Stuhler, P. O. Schmidt, S. Hensler, J. Werner, J. Mlynek, and T. Pfau, "Continuous loading of a magnetic trap," Phys. Rev. A **64**, 031405-1–031405-4 (2003).
12. A. S. Bell, J. Stuhler, S. Locher, S. Hensler, J. Mlynek, and T. Pfau, "A magneto-optical trap for chromium with population repumping via intercombination lines," Europhys. Lett. **45**, 156–161 (1999).
13. C. C. Bradley, J. J. McClelland, W. R. Anderson, and R. J. Celotta, "Magneto-optical trapping of chromium atoms," Phys. Rev. A **61**, 053407-1–053407-6 (2000).
14. B. G. Lindsay, K. A. Smith, and F. B. Dunning, "Control of long-term output frequency drift in commercial dye-lasers," Rev. Sci. Instrum. **62**, 1656–1657 (1991).
15. G. A. Martin, J. R. Fuhr, and W. L. Wiese, "Atomic transition probabilities, scandium through manganese," J. Phys. Chem. Ref. Data **17**, suppl. 3 (1988).
16. J. J. McClelland and M. H. Kelley, "Detailed look at aspects of optical pumping in sodium," Phys. Rev. A **31**, 3704–3710 (1985).
17. W. Jitschin, "Locking the laser frequency to an atomic transition," Appl. Phys. B **33**, 7–8 (1984).
18. In fact, three slightly different load thresholds (1000 s^{-1}, 1020 s^{-1} and 1142 s^{-1}) and four slightly different dump thresholds (7000 s^{-1}, 7200 s^{-1}, 7220 s^{-1} and 7670 s^{-1}) were used for the various runs reported here; however, variation in the performance over these values was observed to be negligible.